Received: 27 December 2024 | Revised: 24 February 2025 | Accepted: 11 March 2025

DOI: 10.1002/alz.70153

Alzheimer's & Dementia®
THE JOURNAL OF THE ALZHEIMER'S ASSOCIATION

RESEARCH ARTICLE

Heterogeneous tau deposition patterns in the preclinical stage link to domain-specific cognitive deficits

Seyed Hani Hojjati[1] | Gloria C. Chiang[1] | Tracy A. Butler[1] | Kewei Chen[2,3,4] | Mohammad Khalafi[1] | Bardiya Ghaderi Yazdi[1] | Nancy Foldi[1] | Siddharth Nayak[5] | Mony de Leon[1] | Yi Li[1] | Yaakov Stern[6,7,8,9] | José A. Luchsinger[10,11] | Qolamreza R. Razlighi[1]

[1]Department of Radiology, Brain Health Imaging Institute, Weill Cornell Medicine, New York, New York, USA

[2]College of Health Solutions, Arizona State University, Phoenix, Arizona, USA

[3]School of Mathematics and Statistics, Arizona State University, Phoenix, Arizona, USA

[4]Department of Neurology, University of Arizona College of Medicine, Tucson, Arizona, USA

[5]Department of Neurology, Albert Einstein College of Medicine, Bronx, New York, USA

[6]Taub Institute for Research on Alzheimer's Disease and the Aging Brain, Vagelos College of Physicians and Surgeons, Columbia University, New York, New York, USA

[7]Department of Neurology, Vagelos College of Physicians and Surgeons, Columbia University, New York, New York, USA

[8]Gertrude H. Sergievsky Center, Vagelos College of Physicians and Surgeons, Columbia University, New York, New York, USA

[9]Department of Psychiatry, Vagelos College of Physicians and Surgeons, Columbia University, New York, New York, USA

[10]Department of Medicine, Columbia University Irving Medical Center, New York, New York, USA

[11]Department of Epidemiology, Columbia University Irving Medical Center, New York, New York, USA

Abstract

INTRODUCTION: The spatial heterogeneity of tau deposition is closely linked to clinical variants of Alzheimer's disease (AD). Detecting these patterns in the preclinical stage is challenging, but second-generation tau tracers provide a unique opportunity to do so.

METHODS: We used independent component analysis (ICA) and tau positron emission tomography (PET) imaging with the 18F-MK6240 tracer in 590 cognitively healthy adults (mean age 66.58 ± 5.13 years, 340 females) to identify tau patterns in the preclinical stage.

RESULTS: Using all individuals, seven distinct patterns emerged, with medial temporal lobe (MTL) involvement associated with age, Aβ burden, apolipoprotein E (APOE) genotype, and plasma total tau. Bilateral amygdala-hippocampus tau deposition was associated negatively with memory ($t = -2.64$, $p < 0.01$), while broader neocortical patterns, especially asymmetric ones, were linked to deficits in language ($t < -3.13$, $p < 0.002$) and reasoning ($t < -2.63$, $p < 0.01$).

DISCUSSION: These findings advance our understanding of preclinical tau heterogeneity, offering new insights for early AD intervention.

KEYWORDS

Alzheimer's disease, domain-specific cognitive deficits, heterogeneous tau deposition, independent component analysis, preclinical stage

Highlights

- Seven tau deposition patterns were identified in preclinical stages of AD, including medial temporal lobe and asymmetric neocortical patterns.

Correspondence
Seyed Hani Hojjati, Department of Radiology, Brain Health Imaging Institute, Weill Cornell Medicine, 401 East 61st Street, Room RR-214, New York, NY 10065, USA.
Email: shh4006@med.cornell.edu

Funding information
National Institute on Aging, Grant/Award Numbers: K24AG045334, 1R01AG057848-01A1, 5R01AG038465-09

- Medial temporal lobe patterns were strongly linked to age, APOE genotype, Aβ burden, and plasma total tau levels.
- Neocortical patterns, especially asymmetric ones, were linked to domain-specific cognitive deficits, notably in language and reasoning.
- This research highlights the potential of using tau deposition patterns for early detection and tailoring interventions in preclinical AD.

1 | Introduction

Alzheimer's disease (AD) is the most common type of dementia, pathologically characterized by the presence of two key features in the brain: β-amyloid (Aβ) plaques and tau tangles.[1–3] Aβ plaques can accumulate in the brain many years or even decades before the onset of noticeable symptoms of AD.[4] While Aβ is essential for a diagnosis of AD[5] and is considered to facilitate the spread of tau,[1,6,7] tau tangles are directly associated with regional brain atrophy and subsequent neurodegeneration.[8] These tangles are closely linked to the loss of cognitive function, leading to deficits in specific domains such as memory and language.[9–11] The relationship between the spatial patterns of tau tangles in the brain and domain-specific decline in cognitive abilities highlights the importance of understanding tau pathophysiology, particularly in the preclinical stages of the disease.

One of the most interesting aspects of tau pathophysiology is its initially localized deposition and highly predictable progression throughout the brain, typically following Braak staging.[12,13] According to Braak staging, the earliest stage of tau pathology emerges in the transentorhinal cortex then spreads to the anterior hippocampus, limbic and temporal cortex, and neocortex, and finally reaches the primary sensory cortex in the latest stages.[12,13] However, emerging evidence suggests that tau aggregation may deviate from the typical Braak staging in specific non-amnestic clinical presentations of AD and may have different domain-specific cognitive declines.[14–16] For instance, when tau deposition occurs predominantly in the parietal and occipital lobes, it often results in deficits in visuospatial processing, leading to a diagnosis of posterior cortical atrophy (PCA).[17,18] Furthermore, patients with focal tau deposition in the left hemisphere commonly display deficits in language and communication skills, clinically diagnosed as logopenic variant primary progressive aphasia (lvPPA).[17,18]

These reports link atypical tau patterns to domain-specific behavioral and cognitive deficits in clinically symptomatic patients.[19–21] However, it is common for cognitively normal individuals to have significant tau deposition[22,23] and whether the pattern of tau deposition is associated with subtle, domain-specific cognitive deficits in this population is unknown. Yet, crucial questions remain unanswered: Can we detect heterogeneous atypical patterns of tau deposition in preclinical populations? If so, what are the associations of these patterns with AD biomarkers and domain-specific cognitive functioning? We hypothesize that cortical tau deposition patterns may have a more disruptive effect on cognitive deficits at preclinical stages than the early-stage patterns involving the medial temporal lobe (MTL) region.

This study utilized independent component analysis (ICA) to identify distinct patterns of tau deposition in the preclinical stages of AD. We employed the largest sample of cognitively normal elderly individuals (n = 590) with the second-generation tau positron emission tomography (PET) tracer (18F-MK6240). The use of 18F-MK6240 tracer enabled us to uncover novel patterns of tau deposition in preclinical stages. The ICA technique successfully identified seven distinct patterns of tau deposition. Additionally, we associated these patterns with (1) age and APOE, (2) Aβ burden and plasma total tau, and more importantly, (3) four neurocognitive domains: language, reasoning, memory, and visuospatial. The research presented here is driven by our passion and recent advancements in working with large-scale imaging datasets, with a particular emphasis on PET imaging, to significantly enhance our understanding of the pathophysiology of the human brain during its preclinical stages.[24–31] Detecting heterogeneous tau patterns and assessing their implications in preclinical stages may help clinicians intervene earlier, potentially delaying or preventing the onset of AD-related cognitive decline.

2 | Materials and Methods

2.1 | Participants

We included 590 healthy old individuals (age 66.58 ± 5.13 years, 340 females) from ongoing studies at Columbia University Irving Medical Center (CUIMC) and the Brain Health Imaging Institute (BHII) at Weill Cornell Medicine (WCM). Table 1 provides a comprehensive summary of the demographics, pathological status, and cognitive assessments. Additionally, Table 2 presents demographic information for a subgroup of individuals from the CUIMC cohort who underwent cognitive assessments across four key domains (language, reasoning, memory, and visuospatial) with information on APOE genotype and plasma total tau. All individuals underwent ^{18}F-MK6240 tau-PET and ^{18}F-Florbetaben Aβ-PET, magnetic resonance imaging (MRI), and evaluations covering medical and neuropsychological assessments. These evaluations confirmed the absence of neurological or psychiatric

disorders, any impairment, and significant medical conditions, indicating that all these individuals function normally in their daily lives. The data used in this study have been reviewed and approved by institutional review boards (IRBs) located at CUIMC and WCM.

2.2 | Neuroimaging

All individuals followed a standardized imaging protocol for tau- and Aβ-PET scans. For tau-PET, individuals received the ^{18}F-MK6240 tracer via an intravenous catheter in the arm, with an injection of 185 MBq (5 mCi) $\pm$ 20% (maximum volume 10 mL), administered as a single IV bolus within 60 s or less (equivalent to 6 secs/mL max). Brain images were acquired starting 90 min after the tracer injection, with six 5-min frames over a duration of 30 min. For Aβ-PET, individuals received the ^{18}F-Florbetaben tracer via an intravenous catheter in the arm, with an injection of 300 MBq (8.1 mCi) $\pm$ 20% (maximum volume 10 mL), administered as a single IV bolus within 60 s or less (equivalent to 6 secs/mL max). Brain images were acquired starting 90 min after the tracer injection with four 5-min frames over a duration of 20 min.

MRI scans at 3T with a 3D volumetric T1 magnetization-prepared rapid gradient-echo sequence were performed. Each participant first underwent a high-resolution T1 image with TR /TE = 2400–3000/2.7–2.9 ms, flip angle = 8–12°, and 176–512 slices with 0.5–1 mm thickness.

2.3 | Image Analyses

The following analyses used our in-house PET processing pipeline.[29,32] First, the individual's MRI was processed using the Freesurfer[33] (http://surfer.nmr.mgh.harvard.edu) automated segmentation and cortical parcellation software package. All PET frames (six frames in tau-PET and four frames in Aβ-PET) are re-aligned to the first frame using rigid-body registration and averaged to obtain a composite volume. Then the composite PET image was registered to the same individual's MRI image in Freesurfer space using normalized mutual information and six degrees of freedom, resulting in a rigid-body transformation matrix. For the tau-PET image, the standardized uptake value (SUV) is calculated for selected regions and then normalized to the cerebellum gray matter to derive the SUV ratio (SUVR). Co-registering the SUVR imaging in native space to the standard space (MNI152) was necessary for conducting ICA. We utilized advanced normalization tools (ANTs)[34] to map the SUVR image from each individual's native space to the MNI152 space. For Aβ-PET, ANTs[34] are used to map the SUV image from each individual's native space to the MNI152 space. Then, we calculated the SUVR by calculating the SUV using the standard cortex mask and normalized to the whole cerebellum mask as outlined by the Global Alzheimer's Association Interactive Network. Quality assurance involved analyses to validate the slope, intercept, and R^2 values of the processed images.[35] Finally, we determined the Centiloid value using the global Aβ SUVR in the cortex mask.

RESEARCH IN CONTEXT

1. **Systematic review**: Tau accumulation is a hallmark of neurodegenerative diseases, particularly Alzheimer's disease (AD). Existing literature underscores the heterogeneity in spatial patterns of tau deposition and their associations with clinical variants of AD. However, studies focusing on the preclinical stages of AD are limited due to the challenges in detecting these patterns early. Second-generation tau tracers, such as 18F-MK6240, have emerged as promising tools for visualizing tau pathology with higher sensitivity and specificity. This study builds on these advancements, employing independent component analysis (ICA) to characterize heterogeneous tau patterns in a large cohort of cognitively healthy individuals.
2. **Interpretation**: We identified seven distinct patterns of tau deposition in preclinical AD using ICA on tau positron emission tomography (PET) imaging. These patterns varied in their spatial distribution and showed differential associations with established AD biomarkers and domain-specific cognitive deficits. We found two patterns involving the medial temporal lobe (MTL) subregions; one involving the bilateral entorhinal cortex, which was most strongly correlated with age, while the other involved the hippocampus and amygdala with a robust association with amyloid-beta (Aβ) burden and memory decline. Additionally, we identified five neocortical tau deposition patterns that were associated with different cognitive declines, particularly language and reasoning. Interestingly, these five neocortical patterns were not significantly associated with age, APOE genotype, plasma total tau, or Aβ burden. This suggests that other underlying mechanisms may drive neocortical tau deposition in cognitively normal individuals.
3. **Future directions**: This study provides a foundation for integrating spatial tau patterns into predictive models of AD progression. Future work should explore longitudinal data to validate these patterns and examine their evolution over time. Additionally, expanding the analysis to include other neurodegenerative conditions may provide broader insights into the role of tau heterogeneity across diseases. Finally, investigating therapeutic interventions targeting specific tau patterns could open new avenues for personalized treatment strategies in preclinical AD.

2.4 | ICA Approach

ICA is a powerful tool utilized extensively in neuroimaging, particularly in functional magnetic resonance imaging (fMRI) data analysis, where it provides dynamic insights into brain activity across different time

TABLE 1 Demographics of the population across two centers.

Parameter	Total ($N = 590$)	CUIMC ($n = 426$)	BHII ($n = 164$)
Age mean (std)	66.58 (5.12)	65.95 (4.54)	68.23 (6.08)
Gender (male/female)	250/340	161/265	89/75
Aβ burden Centiloid mean (std)	−0.01 (25.91)	−6.20 (19.50)	16.04 (32.70)
Aβ status (positive/negative)	85/498	54/372	31/133
Braak stage 1-2 tau regions SUVR mean (std)	0.99 (0.26)	0.99 (0.26)	0.99 (0.21)
Braak stage 3-4 tau regions SUVR mean (std)	0.98 (0.14)	0.98 (0.14)	0.98 (0.13)
Braak stage 5-6 tau regions SUVR mean (std)	0.94 (0.12)	0.93 (0.12)	0.94 (0.11)
Selective reminding test total recall mean (std)	–	41.71 (10.10)	–
Selective reminding test total recall mean (std)	–	6.02 (2.59)	–
Blind MOCA mean (std)	–	–	19.38 (2.09)

Abbreviations: Aβ, βeta-amyloid; BHII, Brain Health Imaging Institute; CUIMC, Columbia University Irving Medical Center; MOCA, Montreal Cognitive Assessment; std, standard deviationSUVR, standardized uptake value ratio.

TABLE 2 Individuals with four domains of cognitive assessment, APOE ε4, ethnicity, and plasma total tau data in the CUIMC cohort.

Parameter	$N = 360$
Age mean (std)	64.96 (3.16)
Gender (male/female)	128/232
Ethnicity (Hispanic/Non-Hispanic White/Non-Hispanic Black)	242/47/71
APOE ε3/4 (positive/negative)	106/230
Plasma total tau mean (std)[a]	2.26 (1.45)
Years of education (std)	11.80 (4.08)
Category fluency mean (std)	45.55 (13.59)
Letter fluency mean (std)	29.05 (12.53)
Selective reminding test total recall mean (std)	40.72 (9.86)
Identities and oddities mean (std)	13.43 (2.19)
Benton Visual Retention Test match score mean (std)	8.59 (2.91)
Benton Visual Retention Test delayed score mean (std)	7.58 (2.92)

Abbreviations: APOE, apolipoprotein E; CUIMC, Columbia University Irving Medical Center; std, standard deviation.
[a]Only 336 of 360 individuals have plasma total tau data.

points.[36–38] In processing single frame (not time series like fMRI) such as tau-PET scans, ICA can be applied to the inter-population volume[39] and decomposed into a mixing matrix (ICA expression) and a source matrix (tau uptake). The mixing matrix captures the relationship between participants and sources, while the source matrix maintains the relationship between sources and brain tau voxels. To conduct the ICA, we first merged individual tau SUVR images in the Montreal Neurological Institute (MNI) 152 template space into a 4D image. Notably, we used all 590 individuals (both Aβ-negative and Aβ-positive). Subsequently, we applied a 2 mm full width at half maximum (FWHM) smoothing to the scans. To optimize the detection of ICs associated with nonspecific binding spill-in from meningeal tissue and skull, commonly observed in 18F-MK4260 tracer scans,[40] we first chose not to exclude meningeal tissue and skull from the tau images. Notably, we also repeated the ICA analysis by excluding the meningeal tissue and skull from the tau images. Following this, we applied MELODIC on the smoothed 4D image. Individual significance within each independent component (IC) pattern was determined by their expression in the mixing matrix. Finally, min–max normalization was applied to each selected IC expression, ranging from 0 to 1, aiding in clearer interpretation and visualization. An IC expression close to 0 indicated minimal individual expression, while an expression near 1 indicated maximal expression within each IC component. Each voxel-wise IC map was displayed with *z*-scores, which quantify how many standard deviations a particular voxel's value deviates from the mean. These *z*-scores were calculated using the mean and standard deviation of all IC maps, providing a clear measure of how much each voxel in each IC map stands out compared to the average across the entire IC maps.

2.5 | Calculation of tau Uptake in IC Maps

To compute the tau uptake within each IC spatial map, we utilized the *z*-scored spatial IC maps generated by the MELODIC output. To limit the spatial overlap across IC maps, we selected a *z*-score threshold of six and binarized the IC maps. Then we calculated the average SUVR in these spatially binarized maps.

2.6 | Global Aβ Burden

To evaluate the Aβ burden, we utilized the Centiloid metric, which utilized an AD-related mean-cortical target mask for all participants. This metric provides a standardized measure for quantifying the global Aβ burden.[35] Additionally, to distinguish between Aβ-positive and Aβ-negative participants, we employed a cut-point of 19.[41]

2.7 | Cognitive Assessments

We characterized the tau deposition patterns with four cognitive domains drawn from six cognitive assessments: language (category fluency, letter fluency), memory (selective reminding total delayed recall), reasoning (identities and oddities), and visuospatial (Benton visual retention test match and delayed score). In summary, the category fluency task assesses semantic verbal fluency by requiring participants to generate as many words as possible from a given category within a set time frame.[42] The letter fluency task evaluates verbal fluency, where participants produce words beginning with a specific letter, assessing executive function and vocabulary retrieval.[43] The selective reminding total delayed recall assessment measures episodic memory and long-term retention through a selective reminding paradigm, requiring recall of a list of items after a delay.[44] Identities and oddities task involves abstract reasoning and problem-solving skills by identifying similarities and differences among items.[45] The Benton visual retention test assesses visuospatial memory, and visual perception by requiring participants to reproduce geometric designs.[46]

2.8 | Statistical Analyses

We organized our statistical analyses into three main categories to provide a comprehensive understanding of the tau patterns observed within each IC:

2.8.1 | Associations Between IC Expressions, Age, and APOE Genotype

Initially, using all 590 individuals, we examined the link between age and each IC map expression. This involved conducting distinct multiple regression analyses for each IC map while adjusting for gender as a covariate (model 1):

$$IC\ expression_i = \beta_0 + \beta_1 \text{Age} + \beta_2 Gender + e \quad (1)$$

where *i* varies between 1 and the maximum number of IC maps.

We then utilized data from the 360 individuals (both Aβ-negative and Aβ-positive) who had available APOE ε3/4 status information to explore the associations with IC map expressions. We conducted multiple regression analyses to provide insight into how the APOE ε3/4 status related to each IC expression (model 2) while controlling for the potential covariates, including age, gender, and ethnicity.

$$IC\ expression_i = \beta_0 + \beta_1 \text{APOE status} + \beta_2 \text{Age} + \beta_3 Gender + \beta_3 Ethnicity + e \quad (2)$$

where *i* varies between 1 to the maximum number of IC maps.

2.8.2 | Associations Between IC Expressions, Aβ Burden, and Total tau

Then, we analyzed the relationships between IC map expressions and Aβ burden, measured using Centiloid, using all 590 individuals. Distinct multiple regression analyses were performed for each IC map to investigate how IC expressions relate to Aβ burden (model 3) while adjusting for age and gender as covariates.

$$IC\ expression_i = \beta_0 + \beta_1 \text{Centiloid} + \beta_2 \text{Age} + \beta_3 Gender + e \quad (3)$$

where *i* varies between 1 and the maximum number of IC maps.

We also conducted pairwise *t*-tests to compare IC expression between Aβ-negative and Aβ-positive individuals. Notably, this analysis strengthens our statistical approach by accounting for potential nonlinear relationships between Aβ and IC expression.

Next, to evaluate the combined effect of Aβ status and age on the expression of each IC map, we conducted an interaction model that adjusted for gender (model 4). This interaction model examines the association of each IC's expression with age and Aβ status, while including an interaction term between Aβ status and age. We aim to capture any differential effects of age on IC expression that may vary by Aβ status.

$$IC\ expression_i = \beta_0 + \beta_1 A\beta\ Status + \beta_2 Age + \beta_3 Age * A\beta\ Status + \beta_4\ Gender + e \quad (4)$$

where *i* varies between 1 and the maximum number of IC maps.

In separate analyses, using data from 336 individuals (both Aβ-negative and Aβ-positive) with plasma total tau information, we conducted multiple regression analyses to evaluate the association between tau IC expression and plasma total tau levels. This was done while adjusting for age, gender, and APOE ε3/4 status (model 5).

$$IC\ expression_i = \beta_0 + \beta_1 \text{total tau} + \beta_2 \text{APOEstatus} + \beta_3 Age + \beta_4 Gender + e \quad (5)$$

where *i* varies between 1 and the maximum number of IC maps.

2.8.3 | Associations between tau deposition in each IC map and cognitive assessments

In our investigation of cognitive assessments, in each tau pattern (IC maps), we focused on individuals with the highest levels of IC expression. To identify these individuals, we first sorted the IC expression of each tau pattern and then selected the top quartile (90 samples) with the highest expression out of 360 individuals who had cognitive assessments in all four domains. This approach ensured that we were analyzing individuals with the highest IC expression levels compared

to the overall sample while maintaining a consistent sample size for our statistical analyses. Subsequently, we measured tau uptake using the same IC map (using *z*-score > 6). First, we performed regression analyses to examine the associations between each IC expression and tau uptake, measured using the same IC map. Next, for each tau pattern, we conducted six multiple regression analyses to explore the relationships between six cognitive assessments and tau uptake in the individuals with the highest IC expression. These analyses controlled for potential confounding factors such as age, gender, and APOE genotype (model 6).

$$Cognitive\ Score_i = \beta_0 + \beta_1 Tau\ uptake_j + \beta_2 \mathrm{APOE} + \beta_3 Age + \beta_4 Gender + e \quad (6)$$

where *i* varies between 1 and 6, and j varies between 1 and the maximum number of IC maps to explore the relationship between six cognitive assessments and tau uptake in these maps.

All *p*-values resulting from our analyses underwent correction for multiple comparisons using the Holm–Sidak method.[47] We used Python for all statistical analyses.

3 | RESULTS

3.1 | Spatial patterns of tau in the preclinical stage

Multivariate exploratory linear optimized decomposition into independent components (MELODIC) automatically estimated 144 independent components (ICs). Each IC's spatial map underwent visual inspection to remove noise-related components and those related to nonspecific binding outside the brain and in white matter, and we selected the seven IC maps. Furthermore, we conducted ICA with different manually selected dimensions (from 100 to 140) and were able to identify almost the same selected ICs across all different ICA runs. We also repeated the ICA analysis while excluding meningeal tissue and skull, resulting in MELODIC identifying 55 ICs automatically. Although most of the ICs remained linked to nonspecific binding, we again were able to identify the most selected seven ICs demonstrating notable stability. Figure 1 illustrates the spatial pattern of the seven IC maps that we have identified by discarding the ICs with expressions mainly concentrated outside the cerebral cortex. The *z*-score in each ICA map is consciously color-coded. Specifically, blue indicates a minimum *z*-score of 6, and red indicates a *z*-score of 15 or higher. Additionally, Figure S1 illustrates the spatial patterns of the seven IC maps with a different threshold, displaying both negative and positive *z*-scores for better clarification of each IC pattern. We found seven distinct tau patterns, three of which are unilateral, with two confined to the right hemisphere and one to the left hemisphere, and four involving bilateral regions. The ICs were numbered based on their prevalence in our study population, with the first IC being the least prevalent and most unique, and the last IC being the most prevalent.

1. Asymmetric right parietal: This pattern includes the inferior parietal, pre- and post-central, precuneus, and supramarginal regions.
2. Asymmetric left frontal-temporoparietal: This tau pattern exhibits greater tau in the left hemisphere, including the temporoparietal, precuneus, and middle frontal regions.
3. Bilateral temporal-occipital: This pattern demonstrates bilateral deposition in the temporal and occipital lobes, with a more pronounced presence on the left hemisphere than the right hemisphere.
4. Asymmetric right frontal-temporal: This pattern appears asymmetric in the right hemisphere, predominantly affecting the temporal lobe and middle frontal areas.
5. Bilateral temporoparietal: This pattern is demonstrated bilaterally in the temporoparietal region.
6. Bilateral amygdala-hippocampus: The sixth pattern is characterized by the unique involvement of bilateral subcortical regions such as the amygdala and hippocampus, and cortical areas like the middle and superior temporal regions.
7. Bilateral entorhinal cortex: The last tau pattern, indicative of the earliest stage of tau uptake, shows bilateral involvement mainly in the entorhinal and fusiform regions.

3.2 | Associations between IC expressions, age, and APOE genotype

Utilizing a total sample of 590 individuals, our study initially investigated the relationship between each IC expression with age (Figure 2). As depicted in Figure 2, out of the seven IC expressions, our analyses revealed that only three IC expressions have a significant association with age: IC3 (bilateral temporal-occipital) with $t = 2.48$, IC6 and $p < 0.013$ (bilateral amygdala-hippocampus) with $t = 3.07$ and $p < 0.002$, and finally IC7 (bilateral entorhinal cortex) with a strong relationship of $t = 5.02$ and $p < 6.69\text{e-}7$. However, only relationships in two patterns involving the MTL (bilateral amygdala-hippocampus and bilateral entorhinal cortex) survived after multiple comparison corrections.

Utilizing a subset of individuals with the information on APOE ε3/4 status (360 samples), our investigation, as illustrated in Figures 3A, B, highlights a distinct relationship between both IC6 and IC7 expressions with APOE ε3/4 status, but not on the other five ICs without any MTL involvement. Specifically, our analysis reveals a significant association between APOE ε3/4 positivity and higher expression of IC6 and IC7, by $t = 3.56$, $p < 0.007$ and $t = 3.02$, $p < 0.003$, respectively. Both associations survived after multiple comparison corrections.

3.3 | Associations between IC expressions, Aβ burden, and plasma total tau

Utilizing a total sample of 590 individuals, Figure 4 shows our analyses of the relationship between Aβ burden (Centiloid) and the seven IC expressions. Our findings highlight only significant relationships between Centiloid global Aβ burden and the IC6 and IC7 expressions. Specifically, IC6 with involvement of the limited cortical brain regions

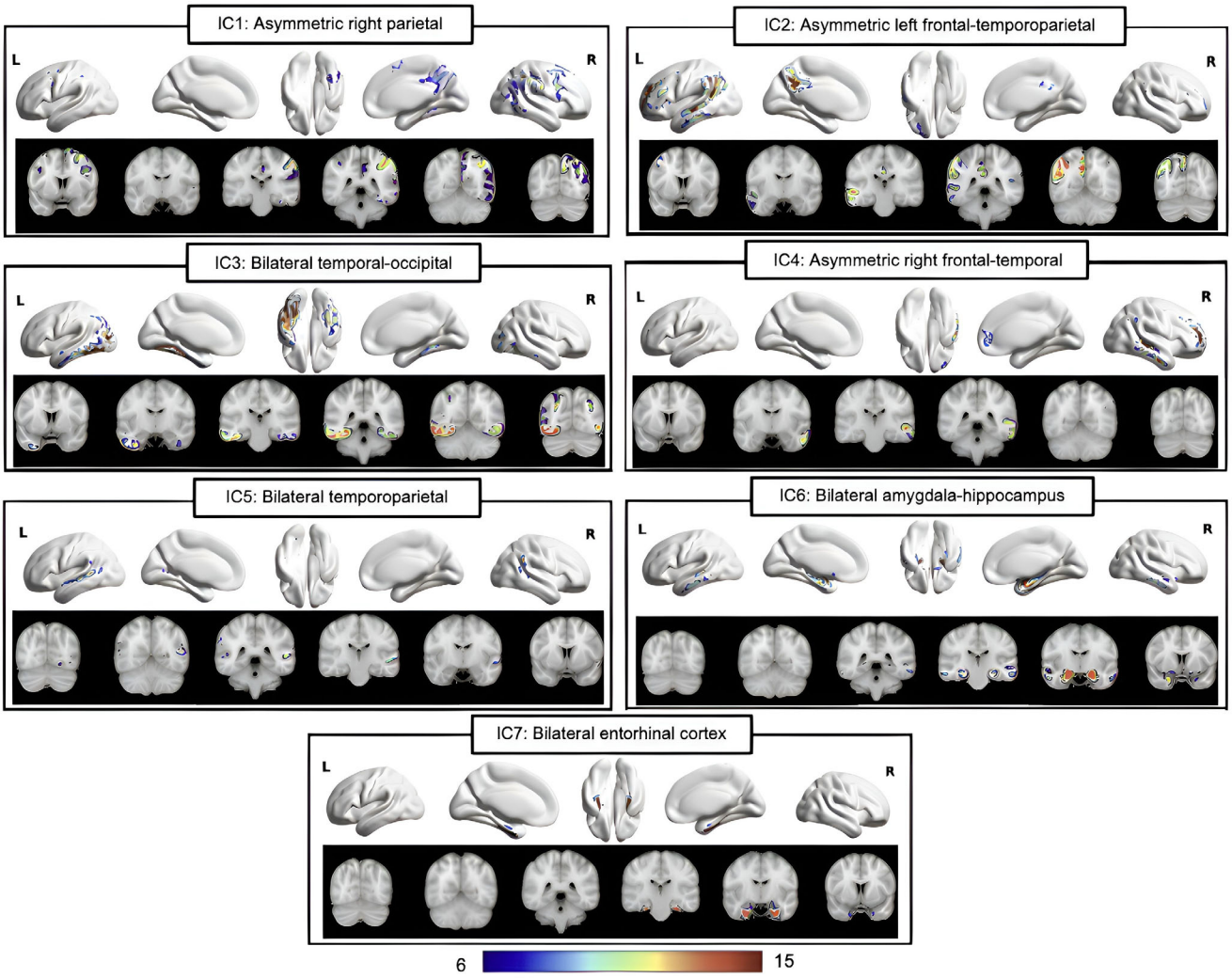

FIGURE 1 Spatial patterns of tau in seven IC maps. The *z*-score in each ICA map is color-coded, with blue indicating a *z*-score of 6 and red indicating a *z*-score of 15 or higher. We found seven distinct tau patterns: IC1: Asymmetric right parietal, IC2: Asymmetric left frontal-temporoparietal, IC3: Bilateral temporal-occipital, IC4: Asymmetric right frontal-temporal, IC5: Bilateral temporoparietal, IC6: Bilateral amygdala-hippocampus, IC7: Bilateral entorhinal cortex. IC, independent component; ICA, independent component analysis.

demonstrates a stronger association compared to IC7, with $t = 4.84$ and $p < 1.6$ e-6. IC7 also showed a significant relationship with Aβ burden, highlighted by $t = 3.71$ and $p < 0.00002$. None of the other IC expressions showed associations with Aβ burden. The pairwise *t*-tests on IC expression between Aβ-positive and Aβ-negative individuals were consistent with the linear regression analyses, showing that Aβ-positive individuals had significantly higher expression of only IC6 ($t = 5.69$, $p < 1.96$ e-8) and IC7 ($t = 5.58$, $p < 3.58$ e-8) compared to Aβ-negative individuals.

Next, we further conducted interaction analyses to examine the potential effect of the interaction between Aβ positivity and age on the expression of IC6 and IC7 (model 4). The results, illustrated in Table 3, indicate that IC6 expression is significantly associated with both age and Aβ positivity ($t > 2.35$, $p < 0.019$). Conversely, in the case of IC7 with bilateral entorhinal cortex involvement, the IC expression demonstrated a highly significant association only with age ($t = 4.05$, $p < 0.00006$) and the association with Aβ attenuates substantially to a statistically insignificant level. The interaction between Aβ positivity and age was not found to be significantly associated with both IC6 and IC7 expressions.

Our examination of plasma total tau levels in Figure S2 closely mirrors the Aβ findings, with only IC6 and IC7 expressions emerging as pivotal patterns showcasing significant associations with total tau. IC6 demonstrates $t = 2.70$ and $p < 0.025$ (not survive after multiple comparison corrections), while IC7 exhibits an association with a $t = 3.50$ and $p < 0.001$.

3.4 | Associations between tau deposition in each IC map and cognitive assessments

Finally, using the top quartile (90 samples) with the highest expression, we investigated the relationship between tau uptake in each IC map and cognitive assessments across four cognitive domains: memory,

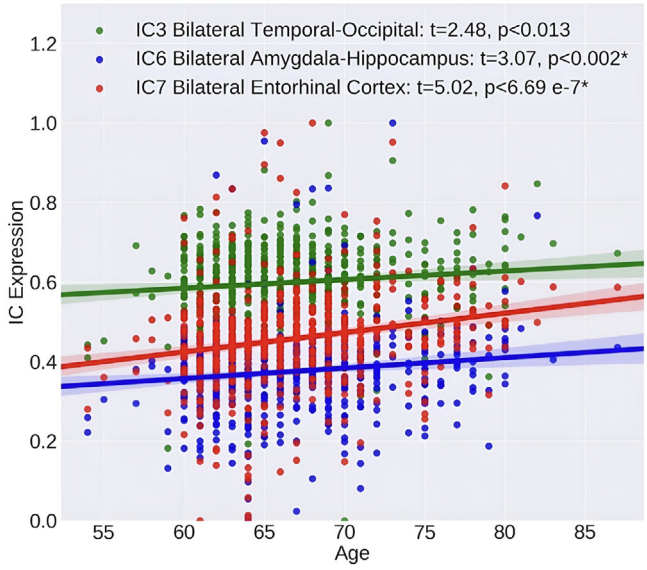

FIGURE 2 Significant relationship between IC3 (bilateral temporal-occipital), IC6 (bilateral amygdala-hippocampus), and IC7 (bilateral entorhinal cortex) expressions with age. *Relationships that remained significant after applying multiple comparison corrections. IC, independent component.

language, reasoning, and visuospatial. The demographics of individuals are illustrated in Table S1. There is no significant difference in demographics, clinical, or behavioral measures between these groups of subjects.

In Figure S3, except for IC1 ($t = 1.40$, $p = 0.163$) and IC5 ($t = 1.56$, $p = 0.123$), all other IC expressions were significantly associated with tau uptake measured using the same IC map ($t > 2.25$, $p < 0.027$). As expected, the most common tau deposition patterns in MTL, IC6, and IC7 exhibited the strongest associations between IC expression and tau uptake on the same map ($t > 19.07$, $p < 5.07\text{e-}33$).

Next, we selected the 90 individuals with the highest IC expression and performed multiple regression analyses to explore the relationships between cognitive assessments in four domains and tau uptake in this subgroup. Our statistical findings, displayed in Table 4, with significant results surviving multiple comparison corrections highlighted in bold font. The significant relationships are further depicted in Figure S4.

In the memory domain, the analysis of the selective reminding test total recalls revealed a significant negative association with tau uptake in two IC maps. Specifically, IC5 tau uptake, with a bilateral temporoparietal pattern ($t = -2.23$, $p < 0.02$), and IC6 tau uptake, with a bilateral amygdala-hippocampus pattern ($t = -2.64$, $p < 0.01$), showed a significant negative association. Notably, only the association with IC6 tau uptake marginally survived (adjusted $p < 0.06$) after multiple comparison corrections (Figure S4a).

In the language domain, for the category fluency test, significant negative associations were observed in three IC maps. IC2 tau uptake, with an asymmetric left frontal-temporoparietal pattern, was strongly associated with reduced semantic language performance ($t = -3.26$, $p < 0.002$). Additionally, significant negative associations were found for IC4 tau uptake, with an asymmetric right frontal-temporal pattern ($t = -2.47$, $p < 0.015$), and IC5 tau uptake, with a bilateral temporoparietal pattern ($t = -3.33$, $p < 0.001$). As shown in Figure S4b and S4c, the associations between category fluency and tau uptake in IC2 and IC5 survived multiple comparison corrections.

The second assessment in the language domain, the letter fluency test, revealed significant negative associations with tau uptake in multiple IC maps. IC2 tau uptake, with an asymmetric left frontal-temporoparietal pattern ($t = -3.14$, $p < 0.002$), IC3 tau uptake, with a bilateral temporal-occipital pattern ($t = -2.24$, $p < 0.027$), IC4 tau uptake, with an asymmetric right frontal-temporal pattern ($t = -2.30$, $p < 0.024$), and IC5 tau uptake, with a bilateral temporoparietal pattern ($t = -3.13$, $p < 0.002$), all demonstrated significant negative associations with phonemic language performance. As shown in Figures S4d and 6e, only the associations between letter fluency and tau uptake in IC2 and IC5 survived multiple comparison corrections.

In the reasoning domain, the identities and oddities test showed significant negative associations with tau uptake in several IC maps, and all these associations survived multiple comparison corrections (Figures S4f, S4g, and S4h). IC1 tau uptake, with an asymmetric right parietal pattern, was negatively associated with reasoning test performance ($t = -2.63$, $p < 0.01$). IC3 tau uptake, with the bilateral temporal-occipital pattern, demonstrates a strong negative relationship ($t = -3.55$, $p < 0.001$), and IC5 tau uptake, with a bilateral temporoparietal pattern, significantly associates with poorer performance ($t = -3.064$, $p < 0.003$).

In the visual retention domain, the Benton visual retention test match score analysis revealed a marginally significant negative association with IC3 tau uptake, with a bilateral temporal-occipital pattern ($t = -2.01$, $p < 0.047$), suggesting a potential link between tau accumulation in this IC map and visuospatial capabilities. However, other ICs did not show significant relationships. In the delayed score analysis, IC5 tau uptake, with a bilateral temporoparietal pattern, exhibited a significant negative association ($t = -2.19$, $p < 0.031$), indicating that higher tau levels in this IC map are associated with poorer delayed visual retention. None of the results in visual retention assessments survived multiple comparison corrections.

4 | DISCUSSION

In this study, we aimed to identify heterogeneous patterns of tau deposition in the brain during the preclinical stages of AD and their implications through known AD biomarkers and domain-specific cognitive assessments. We demonstrated four primary findings. First, typical and atypical patterns of tau deposition could be detected in the preclinical stages of AD and the ICA technique effectively disentangled these patterns even with subthreshold levels in cognitively healthy individuals. Second, we confirm prior reports showing that tau accumulation in the MTL region is associated with age, APOE genotype, Aβ burden, plasma total tau, and memory performance. Third, we identified an IC covering the bilateral entorhinal cortex (IC7), which showed a robust

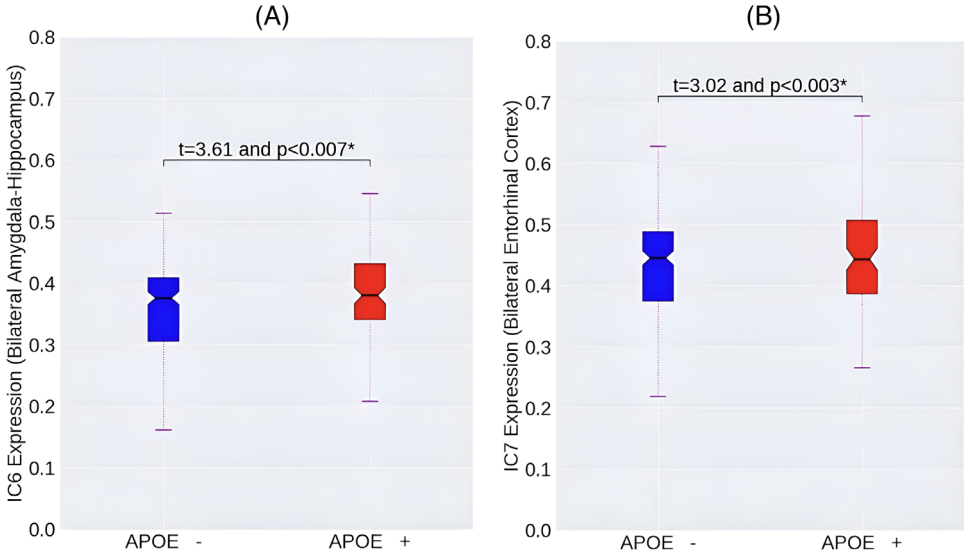

FIGURE 3 Significant relationships between IC6 (bilateral amygdala-hippocampus) and IC7 (bilateral entorhinal cortex) expressions with APOE genotype (A) relationship between APOE ε3/4 status and IC6 expression, and (B) relationship between APOE ε3/4 status and IC7 expression. *Relationships that remained significant after applying multiple comparison corrections. APOE, apolipoprotein E; IC, independent component.

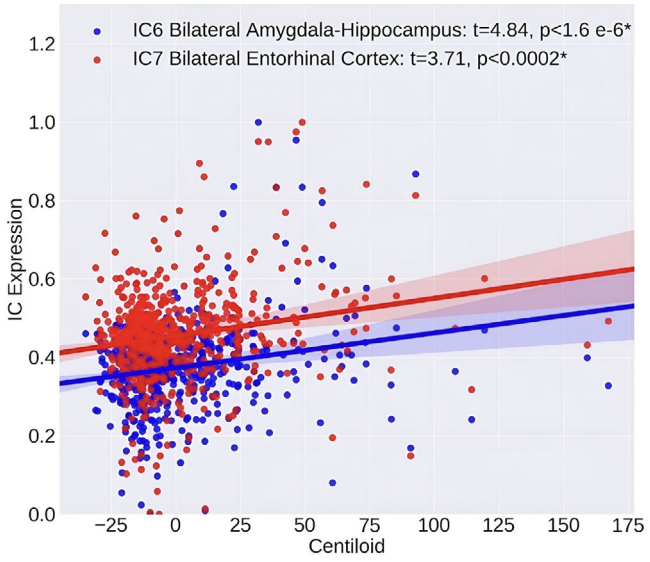

FIGURE 4 The significant relationship between IC6 (bilateral amygdala-hippocampus) and IC7 (bilateral entorhinal cortex) expressions with Aβ burden. *Relationships that remained significant after applying multiple comparison corrections. Aβ, βeta-amyloid; IC, independent component.

association with age. Importantly, the association between this IC and Aβ burden was no longer significant after accounting for Aβ status and its interaction with age. This suggests that IC7 is predominantly age-related, rather than linked to disease pathology. Fourth, unlike the two MTL involvement patterns, the neocortical atypical tau patterns were strongly associated with domain-specific cognitive deficits, especially in language, and reasoning domains. Notably, left-dominated asymmetric tau deposits were highly associated with verbal fluency deficits.

TABLE 3 Interaction results between Aβ status and age.

Model 3: $IC\ expression_i = \beta_0 + \beta_1 A\beta\ status + \beta_2 Age + \beta_3 Age * A\beta\ status + \beta_4 Gender + e$

Tau patterns	Aβ status	Age	Age * Aβ status
IC6 expression	**$t = 2.35$, $p < 0.019$**	**$t = 2.58$, $p < 0.01$**	$t = -1.903$, $p < 0.058$
IC7 expression	$t = 1.45$, $p < 0.14$	**$t = 4.05$, $p < 0.00006$**	$t = -1.058$, $p < 0.291$

Note: Significant relationships are highlighted in bold.
Abbreviations: Aβ, βeta-amyloid; IC, independent component.

Previous quantitative neuroimage studies on tau-PET have primarily focused on validating the Braak staging model for the spread of tau in the brain, which describes the typical progression of tau pathology in AD.[48,49] However, recent studies, particularly those investigating cognitively healthy individuals with Aβ-positive status, have observed positive neocortical tau deposition not conforming to the Braak staging assumption.[22,23] Only a limited number of studies have explored data-driven techniques such as ICA and clustering methods to identify heterogeneous patterns of tau distribution without adhering to predefined spatial distributions.[19–21,50,51] While these prior studies have shed light on various tau deposition patterns beyond the conventional Braak staging model, they mainly focused on clinically symptomatic individuals to detect atypical tau patterns. However, this leaves a significant gap in preclinical research concerning the importance of heterogeneous tau deposition in unimpaired individuals. In one previous study,[52] Young et al. reported that among preclinical Aβ-positive healthy individuals, 9%, out of a population of 392 Aβ-positive individuals, exhibit an atypical tau pattern. These individuals were typically younger, showed reduced cortical thickness in neocortical regions, and

TABLE 4 Relationship between tau uptake in seven IC maps and six cognitive assessments.

Cognitive assessments (neurocognitive domain)	IC1: Asymmetric right parietal	IC2: Asymmetric left frontal-temporoparietal	IC3: Bilateral temporal-occipital	IC4: Asymmetric right frontal-temporal	IC5: Bilateral temporoparietal	IC6: Bilateral amygdala-hippocampus	IC7: Bilateral entorhinal cortex
Selective reminding test total recalls (memory)	NS	NS	NS	NS	$t = -2.23$ $p < 0.02$	***t = −2.64*** ***p < 0.01***[a]	NS
Category fluency (language)	NS	***t = −3.26*** ***p < 0.002***	NS	$t = -2.47$ $p < 0.015$	***t = −3.33*** ***p < 0.001***	NS	NS
Letter fluency (language)	NS	***t = −3.14*** ***p < 0.002***	$t = -2.24$ $p < 0.027$	$t = -2.30$ $p < 0.024$	***t = −3.13*** ***p < 0.002***	NS	NS
Identities and oddities (reasoning)	***t = −2.63*** ***p < 0.01***[a]	NS	***t = −3.55*** ***p < 0.001***	*NS*	***t = −3.064*** ***p < 0.003***	NS	NS
Benton visual retention test match score (visuospatial)	NS	NS	$t = -2.01$ $p < 0.047$	NS	NS	NS	NS
Benton visual retention test delayed score (visuospatial)	N.S	N.S	N.S	N.S	$t = -2.19$ $p < 0.031$	N.S	N.S

Note: Significant relationships after applying multiple comparison corrections are highlighted in bold font.
Abbreviation: IC, independent component; NS, not significant.
[a]Marginally survived after multiple comparison correction.

performed poorly on executive function tasks. Another recent effort[53] by Mishra et al. utilized cluster analysis to identify key regions (e.g., entorhinal cortex, amygdala, occipital lobe) to distinguish between low and high tau binding in preclinical populations. To our knowledge, our study is the first to utilize data-driven methods by employing a second-generation 18F-MK6240 tau tracer to gain a more precise understanding of heterogeneous tau patterns and associated clinical and cognitive associations in preclinical individuals.

We identified two IC maps with distinct patterns with each covering different parts of the MTL, both indicative of typical early-stage patterns. As expected, these patterns were prevalent in our study population, as evidenced by the latest IC maps. This suggests that individuals with higher expression of these two tau patterns in the MTL may develop a typical tau progression. The difference between these MTL-involved patterns lies in the variability across MTL subregions. Specifically, one pattern predominantly involves only the entorhinal cortex, while the other pattern exhibits subcortical involvement such as the amygdala and hippocampus, along with the middle and superior temporal regions. We first confirmed previous reports regarding MTL tau deposition in both patterns, demonstrating a higher prevalence of APOE ε4 carriers,[54,55] and elevated levels of plasma total tau.[56] Crucially, our investigation revealed that the spread of the IC6 tau pattern (amygdala-hippocampus) beyond the MTL is strongly associated with Aβ burden[57] and negatively correlated with memory performance.[58–60] In contrast, the IC7 pattern (predominantly entorhinal cortex) is more closely related to age-associated tau deposition.[61–63] Our findings suggest that, at least in preclinical stages, distinguishing between subregions of MTL is crucial, as each pattern carries different implications.

We identified five distinct neocortical tau deposition patterns, each of which lacks the involvement of MTL subregions. Interestingly, we found no significant association between age, APOE genotype, plasma total tau, and, more importantly, Aβ burden and these neocortical tau patterns. These findings suggest that maybe another underlying mechanism may be driving cortical tau deposition in cognitively normal individuals. Among five neocortical tau patterns, we observed two bilateral patterns with distinct spatial distributions, with one in the temporal-occipital region and the other in the temporoparietal region. Both patterns were associated with deficits in reasoning abilities and language performance and marginally linked to visual processing. The marginally significant findings in the visuospatial domain suggest that, while tau pathology may impact visual processing, its effect might be less noticeable compared to other cognitive domains, which is consistent with prior research.[64] Previous studies[65,66] also highlighted the importance of the frontoparietal and temporal lobes in higher-order cognitive functions such as reasoning tasks. This underscores the significance of the observed neocortical tau deposition patterns and their relationship with cognitive impairment and the distribution of tau pathology in the brain.[65,67,68] The bilateral temporoparietal pattern is also associated with both semantic and phonemic language deficits. The temporal lobe is known for semantic encoding and comprehension of language, lexical retrieval, and the process of accessing.[69,70] Furthermore, previous studies also observed a temporoparietal involvement in individuals with language impairments, suggesting dysfunction in both temporal and parietal areas, including the temporoparietal junction.[71]

Among the seven tau patterns identified in our study, the asymmetric patterns stood out as particularly unique, demonstrating significant clinical relevance. These unique patterns are also well-documented in previous studies including both asymptomatic and symptomatic individuals.[19,72–75] In the current study, we show that the greater tau uptake within the right asymmetric pattern was associated with deficits of reasoning abilities[52] and more importantly asymmetric left

pattern both semantic and phenomics language deficits.[71] Previous research indicated that left hemisphere frontal and temporoparietal regions, especially those involved in language processing, are vulnerable to tau-related disruptions.[76–78] The asymmetric tau patterns, especially in the left hemisphere, are frequently observed in dementia subtypes characterized by more severe language-related symptoms such as in lvPPA of AD and nonfluent/agrammatic variant primary progressive aphasia (nfvPPA) of frontotemporal lobar degeneration (FTLD).[16] lvPPA patients typically exhibit significant uptake across the neocortex, particularly marked in the left temporoparietal region, whereas nfvPPA is notably observed in the left middle and inferior frontal gyri.[16] Both lvPPA and nfvPPA subtypes are characterized by language-related symptoms.

Understanding the reasons behind the heterogeneous tau patterns remains a challenge in the field. However, there are potential explanations for the observed heterogeneous tau patterns. First, it has been hypothesized that brain asymmetry patterns could be linked to alterations in variation in the brain connectome organization.[19] Thus, regions of the brain with higher connectivity and involvement in cognitive assessments may play a more significant role in the spreading of tau.[79–81] Additionally, studies suggested that individuals with temporoparietal and asymmetric tau patterns may have experienced learning difficulties during childhood, potentially influencing cognitive development.[82–84] Despite these explanations, further research is necessary to fully uncover the underlying mechanisms driving tau heterogeneity across the lifespan, especially in the preclinical stage of AD.

This study presents several limitations that require further consideration and may provide opportunities for future investigations. First, the use of second-generation tau tracer, which is relatively new, and the study procedure did not have access to certain biomarkers, such as APOE genotype, plasma total tau, and complete cognitive assessments in some of the participants. However, our analyses included a large number of samples (> 336) to validate the findings. Second, our study dataset was drawn from multiple aging studies, with many individuals in our study population being cognitively and pathologically intact. Nevertheless, including these individuals enhanced the variability in our multivariate technique, which may improve the detection of heterogeneous tau patterns. Lastly, our study reported only the cross-sectional results, and further detailed longitudinal studies are necessary to better interpret the findings.

In conclusion, our study utilized multivariate techniques and a large dataset of tau-PET scans with a second-generation tracer to identify heterogeneous patterns of tau deposition in preclinical individuals. This multivariate approach revealed seven distinct tau patterns within the brain. Our analysis highlighted that tau patterns involving the early-stage MTL were associated with age, Aβ levels, APOE genotype, and elevated plasma total tau levels. Conversely, the asymmetric and bilateral neocortical patterns exhibited a more aggressive and stronger domain-specific association with cognitive deficits, including language and reasoning. The ability to differentiate such heterogeneous patterns in preclinical stages carries significant implications for future clinical trials and the development of targeted interventions.

ACKNOWLEDGMENTS

Our sincere appreciation goes out to all those who played a part in enabling this neuroimaging study to take place. We first express our gratitude to the participants who voluntarily underwent the scanning process, without whom this study would not have been possible. We are grateful for their cooperation, patience, and time invested in the scanning procedures. Finally, we acknowledge all the staff who provided support during the neuroimaging scans. Their professionalism and expertise were invaluable in ensuring the accuracy and reliability of the data. This project used data from studies supported by the National Institute on Aging (K24AG045334, 1R01AG057848-01A1, 5R01AG038465-09).

CONFLICT OF INTEREST STATEMENT

The authors have no Conflict of Interest to report. Author disclosures are available in the Supporting Information.

DATA AVAILABILITY STATEMENT

The data for this project are confidential but may be obtained with Data Use Agreements with Weill Cornell Medicine and Columbia University Irving Medical Center. It can take some weeks to negotiate data use agreements and gain access to the data. The author will assist with any reasonable replication attempts for the following publication.

CONSENT STATEMENT

All human participants provided informed consent.

ORCID

Seyed Hani Hojjati https://orcid.org/0000-0003-3900-9603

REFERENCES

1. Jagust W. Imaging the evolution and pathophysiology of Alzheimer disease. *Nat Rev Neurosci*. 2018;19:687-700.
2. Palmqvist S, Schöll M, Strandberg O, et al. Earliest accumulation of β-amyloid occurs within the default-mode network and concurrently affects brain connectivity. *Nat Commun*. 2017;8:1214.
3. Warren JD, Rohrer JD, Schott JM, Fox NC, Hardy J, Rossor MN. Molecular nexopathies: a new paradigm of neurodegenerative disease. *Trends Neurosci*. 2013;36:561-569.
4. Ghisays V, Lopera F, Goradia DD, et al. PET evidence of preclinical cerebellar amyloid plaque deposition in autosomal dominant Alzheimer's disease-causing Presenilin-1 E280A mutation carriers. *Neuroimage Clin*. 2021;31:102749.
5. Jack CR, Lowe VJ, Weigand SD, et al. Serial PIB and MRI in normal, mild cognitive impairment and Alzheimers disease: implications for sequence of pathological events in Alzheimers disease. *Brain*. 2009;132:1355-1365.
6. Vasconcelos B, Stancu IC, Buist A, et al. Heterotypic seeding of tau fibrillization by pre-aggregated abeta provides potent seeds for prion-like seeding and propagation of tau-pathology in vivo. *Acta Neuropathol*. 2016;131:549-569.
7. Musiek ES, Hotlzman DM. Origins of Alzheimer's disease: reconciling CSF biomarker and neuropathology data regarding the temporal sequence of A-beta and tau involvement. *Curr Opin Neurobiol*. 2012;25:715-720.
8. La Joie R, Visani AV, Baker SL, et al. Prospective longitudinal atrophy in Alzheimer's disease correlates with the intensity and topography of baseline tau-PET. *Sci Transl Med*. 2020;12(524):eaau5732.

9. Reitz C, Honig L, Vonsattel JP, Tang MX, Mayeux R. Memory performance is related to amyloid and tau pathology in the hippocampus. *J Neurol Neurosurg Psychiatry*. 2009;80(7):715-721.
10. Rani N, Alm KH, Corona-Long CA, et al. Tau PET burden in Brodmann areas 35 and 36 is associated with individual differences in cognition in non-demented older adults. *Front Aging Neurosci*. 2023;15:1272946.
11. Bejanin A, Schonhaut DR, La Joie R, et al. Tau pathology and neurodegeneration contribute to cognitive impairment in Alzheimer's disease. *Brain*. 2017;140(12):3286-3300.
12. Braak H, Braak E. Staging of Alzheimer's disease-related neurofibrillary changes. *Neurobiol Aging*. 1995;16(3):271-278.
13. Braak H, Alafuzoff I, Arzberger T, Kretzschmar H, Tredici K. Staging of Alzheimer disease-associated neurofibrillary pathology using paraffin sections and immunocytochemistry. *Acta Neuropathol*. 2006;112(4):389-404.
14. Murray ME, Graff-Radford NR, Ross OA, Petersen RC, Duara R, Dickson DW. Neuropathologically defined subtypes of Alzheimer's disease with distinct clinical characteristics: a retrospective study. *Lancet Neurol*. 2011;10(9):785-796.
15. Whitwell J, Dickson D, Murray M, Petersen R, Jack C, Josephs K. Neuroimaging correlates of pathologically-defined atypical Alzheimer's disease (P05.049). *Neurology*. 2012;78(Meeting Abstracts 1):P05.
16. Roytman M, Chiang GC, Gordon ML, Franceschi AM. Multimodality imaging in primary progressive aphasia. *Am J Neuroradiol*. 2022;43(9):1230-1243.
17. Tetzloff KA, Graff-Radford J, Martin PR, et al. Regional distribution, asymmetry, and clinical correlates of tau uptake on [18F]AV-1451 PET in atypical Alzheimer's disease. *J Alzheimers Dis*. 2018;62(4):1713-1724.
18. Phillips JS, Das SR, McMillan CT, et al. Tau PET imaging predicts cognition in atypical variants of Alzheimer's disease. *Hum Brain Mapp*. 2018;39(2):691-708.
19. Vogel JW, Young AL, Oxtoby NP, et al. Four distinct trajectories of tau deposition identified in Alzheimer's disease. *Nat Med*. 2021;27(5):871-881.
20. Jones DT, Graff-Radford J, Lowe VJ, et al. Tau, amyloid, and cascading network failure across the Alzheimer's disease spectrum. *Cortex*. 2017;97:143-159.
21. Hoenig MC, Bischof GN, Seemiller J, et al. Networks of tau distribution in Alzheimer's disease. *Brain*. 2018;141(2):568-581.
22. Lowe VJ, Wiste HJ, Senjem ML, et al. Widespread brain tau and its association with ageing, Braak stage and Alzheimer's dementia. *Brain*. 2018;141:271-287.
23. Ossenkoppele R, Leuzy A, Cho H, et al. The impact of demographic, clinical, genetic, and imaging variables on tau PET status. *Eur J Nucl Med Mol Imaging*. 2021;48(7):2245-2258.
24. Hojjati SH, Babajani-Feremi A. Seeing beyond the symptoms: biomarkers and brain regions linked to cognitive decline in Alzheimer's disease. *Front Aging Neurosci*. 2024;16:1356656.
25. Hojjati SH, Babajani-Feremi A. Prediction and modeling of neuropsychological scores in Alzheimer's disease using multimodal neuroimaging data and artificial neural networks. *Front Comput Neurosci*. 2022;15:769982.
26. Hojjati SH, Feiz F, Ozoria S, Razlighi QR. Topographical overlapping of the amyloid-β and tau pathologies in the default mode network predicts Alzheimer's disease with higher specificity. *J Alzheimers Dis*. 2021;83:407-421.
27. Hojjati SH, Habeck C, Butler TA, et al. Early accumulation of Aβ and Tau is associated with increase in cortical thickness. *Alzheimers Dementia*. 2022;18(S5):e063715.
28. Hojjati SH, Butler TA, de Leon M, et al. Inter-network functional connectivity increases by beta-amyloid and may facilitate the early stage of tau accumulation. *Neurobiol Aging*. 2025;148:16-26.
29. Hojjati SH, Butler TA, Chiang GC, et al. Distinct and joint effects of low and high levels of Aβ and tau deposition on cortical thickness. *Neuroimage Clin*. 2023;38:103409.
30. Hojjati SH, Chiang GC, Butler TA, et al. Remote associations between tau and cortical amyloid-β are stage-dependent. *J Alzheimers Dis*. 2024;98(4):1467-1482.
31. Hojjati SH, Feiz F, Nayak S, et al. Hub brain regions for the remote spatial association between tau and Amyloid-β proteins. *Alzheimers Dementia*. 2023;19:e076456.
32. Hojjati SH, Butler TA, de Leon M, et al. Between-networks hyperconnectivity is induced by beta-amyloid and may facilitate tau spread. *Medrxiv*. 2024.
33. Fischl B. FreeSurfer. *Neuroimage*. 2012;62:774-781.
34. Avants BB, Tustison N, Song G. Advanced normalization tools (ANTS). *Insight J*. 2009;2(365):1-35.
35. Klunk WE, Koeppe RA, Price JC, et al. The Centiloid project: standardizing quantitative amyloid plaque estimation by PET. *Alzheimers Dementia*. 2015;11:1-15.
36. Varoquaux G, Sadaghiani S, Pinel P, Kleinschmidt A, Poline JB, Thirion B. A group model for stable multi-subject ICA on fMRI datasets. *Neuroimage*. 2010;51(1):288-299.
37. Svensén M, Kruggel F, Benali H. ICA of fMRI group study data. *Neuroimage*. 2002;16(3 Pt 1):551-563.
38. Jenkinson M, Beckmann CF, Behrens TE, Woolrich MW, Smith SM. Fsl. *Neuroimage*. 2012;62(2):782-790.
39. Saha DK, Bohsali A, Saha R, Hajjar I, Calhoun VD. A Multivariate Method for Estimating and comparing whole brain functional connectomes from fMRI and PET data. In *Proceedings of the Annual International Conference of the IEEE Engineering in Medicine and Biology Society*, EMBS; 2023.
40. Jack CR, Wiste HJ, Therneau TM, et al. Associations of amyloid, tau, and neurodegeneration biomarker profiles with rates of memory decline among individuals without dementia. *JAMA*. 2019;321:2316-2325.
41. Jack CR, Wiste HJ, Weigand SD, et al. Defining imaging biomarker cut points for brain aging and Alzheimer's disease. *Alzheimers Dementia*. 2017;13:205-216.
42. Hodges JR, Salmon DP, Butters N. Semantic memory impairment in Alzheimer's disease: failure of access or degraded knowledge?. *Neuropsychologia*. 1992;30(4):301-314.
43. Canning SJD, Leach L, Stuss D, Ngo L, Black SE. Diagnostic utility of abbreviated fluency measures in Alzheimer disease and vascular dementia. *Neurology*. 2004;62(4):556-562.
44. Buschke H. Selective reminding for analysis of memory and learning. *J Verbal Learning Verbal Behav*. 1973;12(5):543-550.
45. Levy G, Jacobs DM, Tang MX, et al. Memory and executive function impairment predict dementia in Parkinson's disease. *Mov Disord*. 2002;17(6):1221-1226.
46. Abe M, Kimura N, Sasaki Y, Eguchi A, Matsubara E. Association between Benton Visual Retention Test scores and PET imaging in elderly adults. *Curr Alzheimer Res*. 2021;18(11):900-907.
47. Narkevich AN, Vinogradov KA, Grjibovski AM. Multiple comparisons in biomedical research: the problem and its solutions. *Ekologiya Cheloveka (Human Ecology)*. 2020;27:55-64.
48. Schöll M, Lockhart SN, Schonhaut DR, et al. PET imaging of tau deposition in the aging human brain. *Neuron*. 2016;89(5):971-982.
49. Cho H, Choi JY, Hwang MS, et al. In vivo cortical spreading pattern of tau and amyloid in the Alzheimer disease spectrum. *Ann Neurol*. 2016;80(2):247-258.
50. Brier MR, Gordon B, Friedrichsen K, et al. Tau and Ab imaging, CSF measures, and cognition in Alzheimer's disease. *Sci Transl Med*. 2016;8(338):338ra66.
51. Whitwell JL, Graff-Radford J, Tosakulwong N, et al. [18F]AV-1451 clustering of entorhinal and cortical uptake in Alzheimer's disease. *Ann Neurol*. 2018;83(2):248-257.

52. Young CB, Winer JR, Younes K, et al. Divergent cortical tau positron emission tomography patterns among patients with preclinical Alzheimer disease. *JAMA Neurol*. 2022;79(6):592-603.
53. Mishra S, Gordon BA, Su Y, et al. AV-1451 PET imaging of tau pathology in preclinical Alzheimer disease: defining a summary measure. *Neuroimage*. 2017;161:171-178.
54. Weigand AJ, Thomas KR, Bangen KJ, et al. APOE interacts with tau PET to influence memory independently of amyloid PET in older adults without dementia. *Alzheimers Dementia*. 2021;17(1):61-69.
55. Young CB, Johns E, Kennedy G, et al. APOE effects on regional tau in preclinical Alzheimer's disease. *Mol Neurodegener*. 2023;18(1):1.
56. Pase MP, Beiser AS, Himali JJ, et al. Assessment of plasma total tau level as a predictive biomarker for dementia and related endophenotypes. *JAMA Neurol*. 2019;76(5):598-606.
57. Hardy JA, Higgins GA. Alzheimer's disease: the amyloid cascade hypothesis. *Science*. 1992;256:184-185.
58. Buckner RL. Memory and executive function in aging and AD: multiple factors that cause decline and reserve factors that compensate. *Neuron*. 2004;44(1):195-208.
59. Yoo HB, Umbach G, Lega B. Neurons in the human medial temporal lobe track multiple temporal contexts during episodic memory processing. *Neuroimage*. 2021;245:118689.
60. Cousijn H, Rijpkema M, Qin S, van Wingen GA, Fernández G. Phasic deactivation of the medial temporal lobe enables working memory processing under stress. *Neuroimage*. 2012;59(2):1161-1167.
61. Crary JF, Trojanowski JQ, Schneider JA, et al. Primary age-related tauopathy (PART): a common pathology associated with human aging. *Acta Neuropathol*. 2014;128:755-766.
62. Wisse LEM, Ravikumar S, Ittyerah R, et al. Downstream effects of polypathology on neurodegeneration of medial temporal lobe subregions. *Acta Neuropathol Commun*. 2021;9(1):128.
63. Leuzy A, Chiotis K, Lemoine L, et al. Tau PET imaging in neurodegenerative tauopathies—still a challenge. *Mol Psychiatry*. 2019;24(8):1112-1134.
64. Prvulovic D, Hubl D, Sack AT, et al. Functional imaging of visuospatial processing in Alzheimer's disease. *Neuroimage*. 2002;17(3):1403-1414.
65. Goel V, Dolan RJ. Explaining modulation of reasoning by belief. *Cognition*. 2003;87(1):B11-B22.
66. Desco M, Navas-Sanchez FJ, Sanchez-González J, et al. Mathematically gifted adolescents use more extensive and more bilateral areas of the fronto-parietal network than controls during executive functioning and fluid reasoning tasks. *Neuroimage*. 2011;57(1):281-292.
67. Seeley WW, Menon V, Schatzberg AF, et al. Dissociable intrinsic connectivity networks for salience processing and executive control. *J Neurosci*. 2007;27(9):2349-2356.
68. Seeley WW, Crawford RK, Zhou J, Miller BL, Greicius MD. Neurodegenerative diseases target large-scale human brain networks. *Neuron*. 2009;62(1):42-52.
69. Carter BT, Foster B, Muncy NM, Luke SG. Linguistic networks associated with lexical, semantic and syntactic predictability in reading: a fixation-related fMRI study. *Neuroimage*. 2019;189:224-240.
70. Binder JR, Frost JA, Hammeke TA, Cox RW, Rao SM, Prieto T. Human brain language areas identified by functional magnetic resonance imaging. *J Neurosci*. 1997;17(1):353-362.
71. Price CJ. A review and synthesis of the first 20 years of PET and fMRI studies of heard speech, spoken language and reading. *Neuroimage*. 2012;62(2):816-847.
72. Sintini I, Martin PR, Graff-Radford J, et al. Longitudinal tau-PET uptake and atrophy in atypical Alzheimer's disease. *Neuroimage Clin*. 2019;23:101823.
73. La Joie R, Visani AV, Lesman-Segev OH, et al. Association of APOE4 and clinical variability in Alzheimer disease with the pattern of tau- and amyloid-PET. *Neurology*. 2021;96(5):e650-e661.
74. Petersen C, Nolan AL, de Paula França Resende E, et al. Alzheimer's disease clinical variants show distinct regional patterns of neurofibrillary tangle accumulation. *Acta Neuropathol*. 2019;138(4):597-612.
75. Ossenkoppele R, Schonhaut DR, Schöll M, et al. Tau PET patterns mirror clinical and neuroanatomical variability in Alzheimer's disease. *Brain*. 2016;139(Pt 5):1551-1567.
76. Gefen T, Gasho K, Rademaker A, et al. Clinically concordant variations of Alzheimer pathology in aphasic versus amnestic dementia. *Brain*. 2012;135(Pt 5):1554-1565.
77. Whitwell JL, Graff-Radford J, Tosakulwong N, et al. Imaging correlations of tau, amyloid, metabolism, and atrophy in typical and atypical Alzheimer's disease. *Alzheimers Dementia*. 2018;14(8):1005-1014.
78. Lu J, Zhang Z, Wu P, et al. The heterogeneity of asymmetric tau distribution is associated with an early age at onset and poor prognosis in Alzheimer's disease. *Neuroimage Clin*. 2023;38:103416.
79. Franzmeier N, Dewenter A, Frontzkowski L, et al. Patient-centered connectivity-based prediction of tau pathology spread in Alzheimer's disease. *Sci Adv*. 2020;6:eabd1327.
80. Franzmeier N, Rubinski A, Neitzel J, et al. Functional connectivity associated with tau levels in ageing, Alzheimer's, and small vessel disease. *Brain*. 2019;142:1093-1107.
81. Franzmeier N, Brendel M, Beyer L, et al. Tau deposition patterns are associated with functional connectivity in primary tauopathies. *Nat Commun*. 2022;13:1362.
82. Miller ZA, Spina S, Pakvasa M, et al. Cortical developmental abnormalities in logopenic variant primary progressive aphasia with dyslexia. *Brain Commun*. 2019;1(1):fcz027.
83. Ossenkoppele R, Rabinovici GD, Smith R, et al. Discriminative accuracy of [18F]flortaucipir positron emission tomography for Alzheimer disease vs other neurodegenerative disorders. *JAMA*. 2018;320(11):1151-1162.
84. Rogalski E, Johnson N, Weintraub S, Mesulam M. Increased frequency of learning disability in patients with primary progressive aphasia and their first-degree relatives. *Arch Neurol*. 2008;65(2):244-248.

SUPPORTING INFORMATION

Additional supporting information can be found online in the Supporting Information section at the end of this article.

How to cite this article: Hojjati SH, Chiang GC, Butler TA, et al. Heterogeneous tau deposition patterns in the preclinical stage link to domain-specific cognitive deficits. *Alzheimer's Dement*. 2025;21:e70153. https://doi.org/10.1002/alz.70153